ICLASS-2006
Aug.27-Sept.1, 2006, Kyoto, Japan

Paper ID ICLASS06-079
SINGLE-COMPONENT LIQUID FILM EVAPORATION MODEL DEVELOPMENT AND VALIDATION USING DIRECT NUMERICAL SIMULATIONS

Gaëtan Desoutter [1], Chawki Habchi [2], Bénédicte Cuenot [3] and Thierry Poinsot [4]

[1]IFP, gaetan.desoutter@ifp.fr
[2]IFP, chawki.habchi@ifp.fr
[3]CERFACS, benedicte.cuenot@cerfacs.fr
[4]CERFACS, thierry.poinsot@cerfacs.fr

ABSTRACT This paper describes a single component liquid film evaporation model. Based on direct numerical simulation (DNS) results of liquid film evaporation in a turbulent channel, new mass, momentum and energy wall laws have been developed in order to take into account the strong gradients of gas density and viscosity near the liquid film, and the gas boundary-layer blowing due to the film evaporation. The liquid film model uses an integral method with a third order polynomial to compute the heat flux inside the liquid film. Moreover, liquid film thermal boundary layer during the transient heating stage is also taken into account. The wall laws and film evaporation model have been implemented in the Reynolds Average Navier-Stokes (RANS) code IFP-C3D. The comparisons of the RANS results with the DNS results are made to substantiate the model presented in this study. The shear stress and heat and mass fluxes at the liquid film interface are reproduced accurately using the new laws of the wall.

Keywords: liquid film, evaporation, wall laws, DNS, RANS, turbulent boundary layer.

1. INTRODUCTION

The phenomena of evaporative liquid film are of relevance to many engineering problems, such as fluid catalytic cracking, ink-jet spray painting, turbine engines, and piston engines. For instance, the environmental standards severization leads the car manufacturers to produce increasingly clean internal combustion engines. The development of direct injection (DI) engines seems to be an interesting solution to reduce the fuel consumption and the emission of pollutants. Unfortunately, for such small engines, most of the time, the fuel spray impinges on the piston surface directly and may forms a liquid film which is one of the most important source of unburned hydrocarbon (HC) and soot production especially during cold start.

Some previous direct numerical simulations (DNS) of liquid film/flame interaction has highlighted that combustion often proceeds in very rich zones leading to the extinction of the flame by smothering [1]. It is then necessary to control the mixture very well and thus the liquid film evaporation if we want to understand the source of HC and soot for DI engines.

Many multidimensional numerical models of liquid film have been previously developed by Stanton & Rutland [2,3], Bai & Gosman [4], Foucart & al [5-6], Han & Xu [7], and O'Rourke & Amsden [8,9] (referred to subsequently as OA). The first three models describe the dynamics of the liquid by an Eulerian approach whereas the OA model adopts a Lagrangian particle tracking method, improved by Han & Xu with a new statistical treatment introduced for the momentum exchange between the impinging spray and the wall film.

The prediction of mass, momentum and heat transfer in the turbulent gas boundary layer above the liquid film is based on correlations using the Sherwood and the Nusselt number [2-4], or wall laws [5-9]. For former case, the main drawback of the correlations is their lack of generality. For the latter case, the models explicitly account the Stephan flow velocity due to the film evaporation. However, they use many assumptions such as gas incompressibility and a simple diffusion of the species model which may lead to inaccurate results. Moreover, for these wall laws, the transition between the fully turbulent region and the viscous laminar sub-layer is assumed to occur at a constant value and independent of the rate of evaporation.

In this paper, a model of liquid film evaporation which better takes into account the blowing velocity due to evaporation, and the strong density and viscosity gradients near the liquid film is presented. These effects will be shown to play an important role on the diffusive transport of momentum, mass and energy in the boundary layer.

In this work, the DNS are used to develop the liquid film evaporation model presented in this study, as well as to check its validity, as the experimental data of liquid film evaporation are rare.

This paper is organized in three sections. In the first one, the DNS performed with the AVBP code [10] are described. Next, the results are discussed and new mass, momentum and energy laws of the wall are established. In the second section, the equations governing the liquid film evaporation model and their implementation in the RANS code IFP-C3D [17] are presented. In the last section, the methodology and the configuration of the model validation are described. Finally, the simulations results are validated by thorough comparisons with the DNS results and the OA model results as well.

2. DNS CALCULATIONS

2.1 DNS Description

DNS code: All the DNS of the present study have been carried out with the AVBP code [10] which uses cell-vertex finite-volume techniques and solves the compressible Navier-Stokes equations on arbitrary unstructured grids for the conservatives variables (mass density, momentum and total energy). It is fully parallelised, dedicated to DNS and Large Eddy Simulations (LES). The numerical scheme used is the TTGC scheme [12] that is third order in time and space.

Computation characteristics: a sketch of the computational domain and the coordinate system is shown in Figure 1. It corresponds to the so-called "minimal channel flow" configuration of Jiménez and Moin [13]. The dimensions of the domain are $L_x = \pi h$, $L_y = 2h$ and $L_z = 0.3\pi h$ in the streamwise, normal and spanwise directions respectively, where h denotes the channel half-width. The top and bottom boundaries of the computational box are liquid film surfaces. The boundaries in both the streamwise x and the spanwise z directions are periodic. The liquid film is made of pure heptane whereas the gas flow consists of an inhomogeneous mixture of air and heptane.

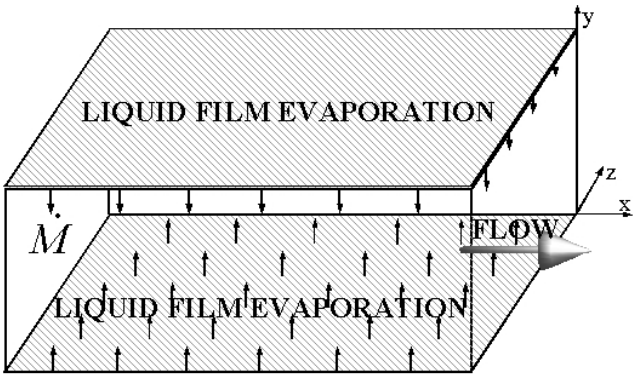

Figure 1: Computational domain for the DNS. The simulations are periodic in both the x and z directions.

The computational grids used are regular in x,z directions with a resolution $\Delta x^+ \approx 35$ and $\Delta z^+ \approx 5$, in order to resolve the expected elongated structure of the turbulence. The non-dimensional coordinates x^+, y^+, z^+ are defined using the characteristic length scale $\nu_{g,s}/u_\tau$ where u_τ and $\nu_{g,s}$ are respectively the shear velocity and the laminar kinematical viscosity of the gas at the liquid film surface.

$$x_i^+ = \frac{x_i u_\tau}{\nu_{g,s}} \ , \ y_i^+ = \frac{y_i u_\tau}{\nu_{g,s}} \ \text{ and } \ z_i^+ = \frac{z_i u_\tau}{\nu_{g,s}} \qquad (1)$$

Grid stretching is used in the normal direction y because the grid spacing near the film needs to be small enough to resolve the viscous sublayer. $\Delta y^+ \leq 1$ is specified near the film surface and $\Delta y^+ \approx 5$ near the centreline of the channel.

Since the DNS inlet and outlet boundary conditions are periodic, our approach consists in adding source terms to the momentum, energy and heptane mass conservation equations in order to compensate for the mean shear stress, heat flux and mass evaporation at the liquid-gas interface. This method has been introduced by Jiménez & Moin [13] for a non-evaporating DNS of the "minimum channel flow".

Since the main objective of our DNS is to build wall laws, it is necessary to reach a stationary state. The liquid film is then modelled as a thin isothermal interface boundary on which the temperature T_s and the mass fraction Y_k^s of each species k are specified. Moreover, the evaporated mass flow of heptane $\dot{M}$, is expressed as follows [14]:

$$\begin{aligned} \dot{M} &= \frac{\rho_{g,s} Y_F^s V_F^s}{1 - Y_F^s} \\ &= \frac{\rho_{g,s} Y_F^s}{1 - Y_F^s} \left[-\frac{D_F^s}{W_s Y_F^s} \left(\frac{\partial W Y_F}{\partial y} \right)_s + \sum_{k=1}^{Nspec} \frac{D_k^s}{W_s} \left(\frac{\partial W Y_k}{\partial y} \right)_s \right] \end{aligned} \qquad (2)$$

where V_F^s and $\rho_{g,s}$ are respectively the diffusion velocity of heptane in y direction and the gas density, both at the liquid-gas interface. $Nspec$ and W denote respectively the number of species in the mixture and the mean molecular weight of the mixture. The laminar mixture diffusion coefficient for species k, D_k, is given by the following approximation :

$$D_k = \frac{\nu_g}{S_{c,k}} \qquad (3)$$

where the laminar Schmidt number for each species k, $S_{c,k}$, is assumed to be constant in time and space.

Reference DNS case: we have performed several DNS with different liquid film surface temperature T_s and heptane's mass fraction Y_F^s corresponding to various evaporation rates. The different parameters given in Tables 1 and 2 summarize the boundary conditions and the main characteristics of the reference DNS case presented in this paper. All quantities with an over bar represent the mean values in both (x,z)-plane and time. The index c denotes the centreline of the channel. $\mathrm{Pr}\,l$ and Re are respectively the

laminar Prandlt number and the Reynolds number of the flow based on the height of the channel.

Table 1: Liquid film surface boundary conditions used in the reference DNS case.

$T_s = 333K$	$Y_F^s = 0.6040$	$Y_{O_2}^s = \frac{1-Y_F^s}{4.29}$
$Y_{N_2}^s = 1-Y_F^s-Y_{O_2}^s$	$v_s = \frac{\dot{M}}{\rho_{g,s}}$	$u_s = w_s = 0$

Table 2: Characteristic parameters defining the reference DNS case.

$h = 1,5612.10^{-3} m$	$\overline{u}_c = 51.69 m.s^{-1}$	$\mathrm{Re} \approx 2700$
$\overline{Y}_{F,c} \approx 0.19$	$\overline{Y}_{O_2,c} \approx 0.19$	$\overline{Y}_{N_2,c} = 0.62$
$\overline{T}_c = 503.69K$	$\overline{P}_c = 99750Pa$	$\mathrm{Pr}\, l = 0.78$
$S_{c,F} = 1.4$	$S_{c,N_2} = 0.4$	$S_{c,O_2} = 0.45$

2.2 Wall Laws Above an Evaporating Liquid Film

The DNS mean profiles of velocity, temperature and species mass fractions has been first plotted as function of classical wall units [13]. The results show that the behavior of the obtained wall laws does not remain logarithmic in the fully turbulent region of the boundary layer above an evaporating liquid film. However, it can be shown that the classical logarithmic behavior may be obtained if the wall laws are expressed using the following variables :

$$U_{eff}^+ = \frac{2}{v_s^+}\left[\sqrt{1+u^+ v_s^+} - 1\right] \tag{4}$$

$$T_{eff}^+ = \frac{2C_T \,\mathrm{Pr}\, t}{v_s^+}\left[\left(1+T^+ v_s^+\right)^{1/2C_1 \mathrm{Pr}\, t} - 1\right] \tag{5}$$

$$Y_{F\,eff}^{\ +} = \frac{2C_Y Sct}{v_s^+}\left[\left(\frac{\overline{Y}_F - 1}{Y_F^s - 1}\right)^{1/2C_2 Sct} - 1\right] \tag{6}$$

where C_T and C_Y are constant given by the comparison between the wall laws and the DNS. $\mathrm{Pr}\, t = 0.9$ and $Sct = 0.9$ denote respectively the turbulent Prandlt and Schmidt number [11]. u^+, v_s^+ and T^+ are defined as follow:

$$u^+ = \frac{\overline{u} - u_s}{u_\tau} \tag{7}$$

$$v_s^+ = \frac{\overline{v}_s}{u_\tau} \tag{8}$$

$$T^+ = -\frac{\left(\overline{T} - T_s\right)\rho_{g,s} C_p u_\tau}{\varphi_{g,s}} \tag{9}$$

where C_p and $\varphi_{g,s}$ are respectively the mass specific heat capacity at constant pressure and the heat flux between the gas flow and the film at the liquid-gas interface.

In order to take into account the compressibility of the gas and the gradients of viscosity, we associate the variables defined by Eq. (4) to (6) with the LnKc model [15] to obtain the following variables:

$$d\eta^+ = \frac{\nu_{g,s}}{\nu_g} dy^+ \tag{10}$$

$$d\varphi_{eff}^+ = \frac{\rho_g}{\rho_{g,s}} du_{eff}^+ \tag{11}$$

$$d\vartheta_{eff}^+ = \frac{\rho_g}{\rho_{g,s}} dT_{eff}^+ \tag{12}$$

$$d\zeta_{eff}^+ = \frac{\rho_g}{\rho_{g,s}} dY_{F\,eff}^{\ +} \tag{13}$$

where ρ_g and ν_g are the local density and laminar kinematical viscosity in the gas.

The wall laws for the fully turbulent region of the boundary layer are finally obtained by substituting the variables η^+, φ_{eff}^+, ϑ_{eff}^+ and ζ_{eff}^+ in the solutions of the RANS equations expressed with the variables y^+, U_{eff}^+, T_{eff}^+, $Y_{F\,eff}^{\ +}$. For the laminar region of the boundary layer, we assume a linear variation of φ_{eff}^+, ϑ_{eff}^+ and ζ_{eff}^+ with the adimensional distance from the liquid film interface η^+. This assumption will be verified in the next subsection using the DNS results.

These laws of the wall are summarized as follow:

$$\begin{cases} \eta^+ \le \eta_l^+ : \varphi_{eff}^+ = \eta^+ \\ \eta^+ \ge \eta_l^+ : \varphi_{eff}^+ = \eta_l^+ + \dfrac{C_u}{k}\ln\left(\dfrac{\eta^+}{\eta_l^+}\right) \end{cases} \tag{14}$$

$$\begin{cases} \eta^+ \le \eta_{l,T}^+ : \\ \vartheta_{eff}^+ = \Pr l \, \eta^+ \\ \eta^+ \ge \eta_{l,T}^+ : \\ \vartheta_{eff}^+ = \Pr l \, \eta_{l,T}^+ + \dfrac{C_u C_T \Pr t}{k} \left[\dfrac{1 + \dfrac{v_s^+ \eta_{l,T}^+}{2C_T} \dfrac{\Pr l}{\Pr t}}{1 + \dfrac{v_s^+ \eta_{l,T}^+}{2}} \right] \ln\left(\dfrac{\eta^+}{\eta_{l,T}^+} \right) \end{cases} \quad (15)$$

$$\begin{cases} \eta^+ \le \eta_{l,m}^+ : \\ \zeta_{eff}^+ = Scl \, \eta^+ \\ \eta^+ \ge \eta_{l,m}^+ : \\ \zeta_{eff}^+ = Scl_t \, \eta_{l,m}^+ + \dfrac{C_u C_Y Sct}{k} \left[\dfrac{1 + \dfrac{v_s^+ \eta_{l,m}^+}{2C_Y} \dfrac{Scl_t}{Sct}}{1 + \dfrac{v_s^+ \eta_{l,m}^+}{2}} \right] \ln\left(\dfrac{\eta^+}{\eta_{l,m}^+} \right) \end{cases} \quad (16)$$

where η_l^+, $\eta_{l,T}^+$ and $\eta_{l,m}^+$ are the distances from the liquid film surface to the laminar-turbulent transition, respectively, for the dynamic, the thermal and the fuel mass fraction boundary layer. Their values are given by the DNS and depends on the evaporation rate (i.e. on the Stefan flow velocity, v_s^+) and the density gradients near the film surface. C_u is a constant given by the comparison between the wall laws and the DNS results. $k = 0.433$ denotes the Karmann's constant [11]. Scl is the laminar Schmidt number of the fuel in the air-heptane mixture, corrected in order to take into account the complex diffusion of the species while using a simple diffusion model. The Scl expression is obtained by identifying $\dot{M}$ given by Eq. (2) and the following Eq. (17).

$$\dot{M} = -\frac{\rho_{g,s} \nu_{g,s}}{\left(1 - Y_F^s\right) Scl} \left(\frac{\partial Y_F}{\partial y} \right)_s \quad (17)$$

The result is given as follow:

$$Scl = W \left[\frac{1 - \overline{Y}_F}{S_{c,F} W_{air}} + \frac{\overline{Y}_F}{S_{c,N_2} W_F} \right] \quad (18)$$

where, W, W_{air}, W_F are respectively the mean molecular weight of the gas mixture, air and fuel. Scl_t is the value of Scl at the laminar-turbulent transition position. Finally, one can note that in the limit of small evaporation rate and gradients of density and viscosity, the wall laws given by Eq. (14) to (16) reduce to the standard wall functions [16].

2.3 Wall Laws Fitting using the DNS Results

Figures 2,3 and 4 show the comparisons between the DNS profiles and the wall laws given by Eq. (14) to (16) for respectively φ_{eff}^+, ϑ_{eff}^+ and ζ_{eff}^+. The values of the constants used in order to adjust the wall functions to the present DNS results are summarized in the Table 3. Except for the buffer zone of the boundary layer, the new walls laws are very close to the DNS results. The assumption of linear evolution in the laminar zone close to the liquid film is very well verified and a logarithmic behavior is observed in the fully turbulent zone.

Table 3: Constants of the wall laws.

$\eta_l^+ = 14.4$	$\eta_{l,T}^+ = 16.3$	$\eta_{l,m}^+ = 12.8$
$C_u = 0.972$	$C_T = 1.257$	$C_Y = 1.023$

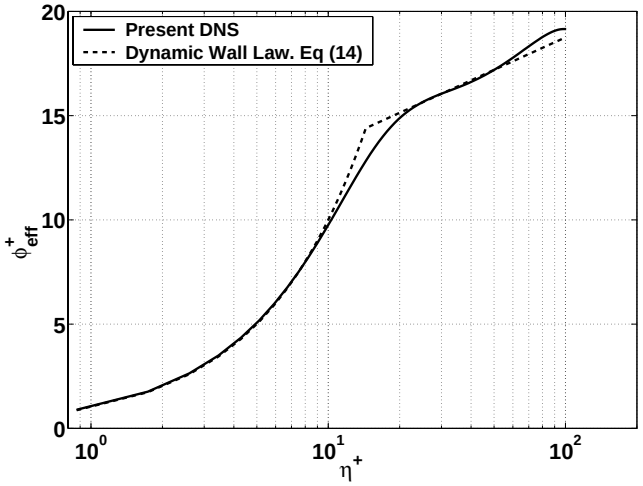

Figure 2: Mean streamwise velocity expressed with $\left(\varphi_{eff}^+, \eta^+\right)$.

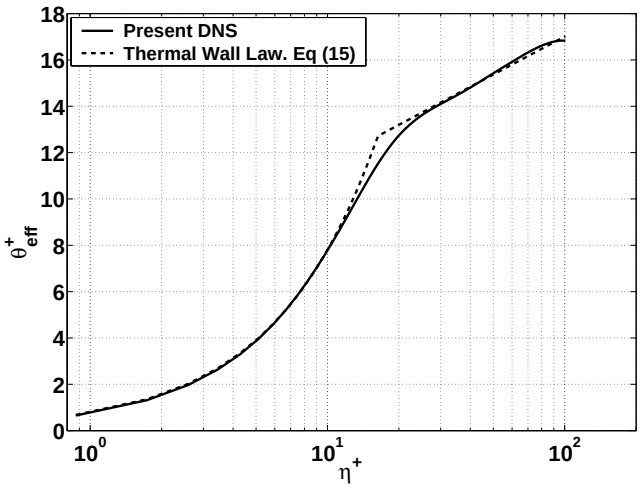

Figure 3: Mean temperature expressed with $\left(\vartheta_{eff}^+, \eta^+\right)$.

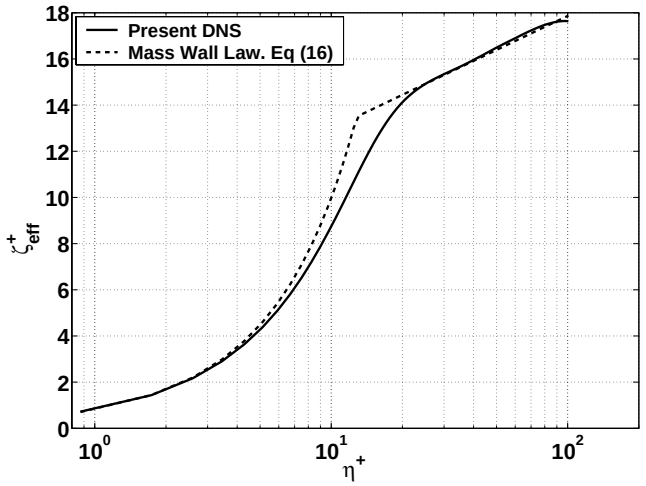

Figure 4: Mean fuel mass fraction expressed with $\left(\zeta^+_{eff}, \eta^+\right)$.

We have noted with different DNS results (carried out in this work and not presented in this paper for lack of space) that these constants depends significantly on the evaporation rate and the density gradients. Correlations of the former parameters to the evaporation data and the thermodynamic conditions are then needed. This is going to be done in future work.

In a general way, the laminar-turbulent transition η_l^+ with evaporation and gradients of density is rather different from the classical critical value of $y^+_{crit} \approx 11$, well known for an isothermal boundary layer above nonvaporizing surfaces. Moreover, the DNS show that the dimensional value of the transition location y_l is always greater than y_{crit}. Indeed, the structure of the boundary layer is modified due to the film evaporation and to the strong gradients of density and viscosity, both decreasing the friction velocity u_τ. For example, an 80% decrease of the friction velocity u_τ has been observed in our reference DNS case ($u_\tau = 1.52$) relatively to an isothermal DNS case ($u_\tau = 2.75$) computed using the same Reynolds number Re and mean streamwise velocity $\overline{u}_c$ in the centerline of the channel.

3. LIQUID FILM EVAPORATION MODEL

3.1 Equations of the Model

In this subsection, we only focus on the energy equation of the liquid film. The generic equation of the mean internal energy of the liquid film $\left\langle \overline{e}_l \right\rangle = C_{vl} \left\langle \overline{T}_l \right\rangle$ can be written as follow:

$$\frac{D}{Dt}\left[\rho_l \left\langle \overline{e}_l \right\rangle h_f S\right] = \dot{Q}_l + \int \left[-\dot{M} \left\langle \overline{e}_l \right\rangle + \varphi_{l,w} - \varphi_{l,s}\right] ds \tag{19}$$

where ρ_l and C_{vl} are respectively the liquid density and the specific heat coefficient at constant volume. This equation was written using a control volume defined by its thickness h_f and area S on the wall. $\dot{Q}_l$ denotes the internal energy brought to film by the impact of the liquid spray droplets by unit time. This term can be found in the bibliography [5-6],[8-9]. $\varphi_{l,w}$ and $\varphi_{l,s}$ are the diffusive heat flux in the liquid, respectively at the wall and at the liquid-gas interface. We focus on these terms in the rest of this subsection as they are of primary importance for the liquid film evaporation model.

$\varphi_{l,s}$ is given by the continuity of heat flux at the liquid-gas interface:

$$\varphi_{l,s} = \varphi_{g,s} + \dot{M} L_V \tag{20}$$

where L_V is the latent heat of vaporization at the film interface T_s. In order to calculate $\varphi_{l,w}$ and T_s, we assume a third order polynomial expression for the temperature profile through the liquid normal direction to the wall $\overline{T}_l(y)$. The mean liquid temperature $\left\langle \overline{T}_l \right\rangle$ defined as follow

$$\left\langle \overline{T}_l \right\rangle = \frac{1}{h}\int_0^{h_f} \overline{T}_l(y) \tag{21}$$

is the solution of Eq. (19). Two cases should be distinguished according to whether the transient heating stage is completed (as shown in Figure 5) or not (as shown in Figure 6).

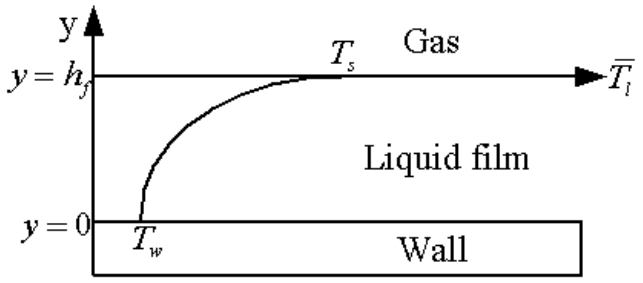

Figure 5: Temperature profile of the liquid film when global heat penetration distance $\delta_l = h$.

If the heat penetration in the liquid film is completed (Figure 5), $\varphi_{l,w}$ and T_s are given by:

$$\varphi_{l,w} = \frac{1}{5}\left[12\frac{\left(T_w - \left\langle \overline{T}_l \right\rangle\right)\lambda_l}{h_f} - \varphi_{l,s} \right] \quad (22)$$

$$T_s = \frac{\left[8\left\langle \overline{T}_l \right\rangle - 3T_w - \frac{h_f}{\lambda_l}\varphi_{l,s} \right]}{5} \quad (23)$$

where T_w and λ_l are the wall temperature and the thermal conductivity of the liquid.

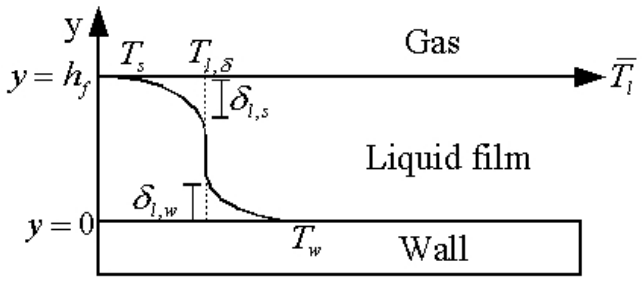

Figure 6: Temperature profile of the liquid film when global heat penetration distance $\delta_l = \delta_{l,s} + \delta_{l,w} < h$.

If the transient heating stage in the liquid film is not completed (Figure 6), $\varphi_{l,w}$ and T_s are given by:

$$\varphi_{l,w} = \frac{3}{2}\lambda_l \frac{\left(T_w - T_{l,\delta}\right)}{\delta_{l,w}} \quad (24)$$

$$T_s = T_{l,\delta} + \frac{4}{3}\alpha\sqrt{\frac{\left(T_{l,\delta} - \left\langle \overline{T}_l \right\rangle_{\delta_s}\right)\varphi_{l,s}h_f}{\lambda_l}} \quad (25)$$

where $T_{l,\delta}$ is the liquid film temperature not achieved by heat penetration (assumed to be constant). α denote the sign of $\varphi_{l,s}$. $\left\langle \overline{T}_l \right\rangle_{\delta_s}$ is the mean liquid temperature if the heat penetration only comes from the film interface. This temperature is given by Eq. (19) with $\varphi_{l,w} = 0$. $\delta_{l,w}$ and $\delta_{l,s}$ are respectively the distance of heat penetration from the wall and from the liquid-gas interface, and are given by:

$$\delta_{l,w} = \frac{8h_f\left(\left\langle \overline{T}_l \right\rangle_{\delta_w} - T_{l,\delta}\right)}{3\left(T_w - T_{l,\delta}\right)} \quad (26)$$

$$\delta_{l,s} = \frac{3\lambda_l\left(T_{l,\delta} - T_s\right)}{2\left(\dot{M}L_V + \varphi_{gs}\right)} \quad (27)$$

where $\left\langle \overline{T}_l \right\rangle_{\delta_w}$ is the mean liquid temperature if the heat penetration only comes from the wall. This temperature is given by Eq. (19) with $\varphi_{l,s} = 0$.

3.2 Model Implementation in IFP-C3D

First of all, the variables defined in Eq. (10) to Eq. (13) are difficult to implement in a RANS code. Instead, we use the following definitions:

$$\eta^+ = f\left(\frac{\nu_{g,s}}{\langle\nu\rangle}\right)y^+ \quad (28)$$

$$\varphi^+_{eff} = P\left(\frac{\langle\rho\rangle}{\rho_{g,s}}\right)u^+_{eff} \quad (29)$$

$$\vartheta^+_{eff} = P\left(\frac{\langle\rho\rangle}{\rho_{g,s}}\right)T^+_{eff} \quad (30)$$

$$\zeta^+_{eff} = P\left(\frac{\langle\rho\rangle}{\rho_{g,s}}\right)Y^{\ +}_{F\,eff} \quad (31)$$

where $\langle\rho\rangle$ and $\langle\nu\rangle$ denote the space averaged density and viscosity along y^+. P and f are respectively a polynomial and a power law, adjusted using DNS results so that the variables defined in Eq.(28) to (31) are equivalent to those defined in Eq. (10) to Eq. (13).

Secondly, in order to improve the accuracy of the model and to decrease the mesh dependence of the results, the wall laws are implemented by numerically integrating the profiles of gas temperature and fuel mass fraction given by Eq. (15) and (16) in the wall cell above the film, by resolving the following equations:

$$\left\langle \rho C_p \overline{T} \right\rangle_m = \frac{1}{L}\int_0^L \rho(y)C_p(y)\overline{T}(y)dy \quad (32)$$

$$\left\langle \rho \overline{Y}_F \right\rangle_m = \frac{1}{L}\int_0^L \rho(y)\overline{Y}_F(y)dy \quad (33)$$

where, $\left\langle X \right\rangle_m$ and L denote the RANS mean value of a variable X in the wall cell and its length in the normal direction to the wall.

Thirdly, the equations Eq. (14-16), Eq. (18-20), Eq. (22-27) and Eq.(32-33) presented in this paper are coupled each other and resolved using an Newton iterative method to improve the stability and accuracy of the numerical scheme.

4. VALIDATION OF THE MODEL

4.1 Methodology

As we did not find experimental data allowing to validate the whole model, a partial validation has been done for the wall laws described in section 2.2. We use the DNS results of the reference case (cf section 2.1) to check the RANS results obtained using IFP-C3D.

The choice of the RANS configuration which provides results comparable with those of the DNS is not obvious. The approach adopted consists in computing a similar channel to that we have used in the DNS calculations. The configuration is given in Figure 7. The computational grid used is regular in all the directions with (192 x 8 x 1) cells in order to have the upper part of the wall cells in the fully turbulent region of the boundary layer ($\Delta\eta^+ \approx 21.5$). For the the channel inlet boundary conditions a flat profile of velocity, temperature and mass fraction of heptane, azote and oxygen, are specified. On the other hand, a pressure boundary condition $\overline{P}_{out}$ is specified at the channel exit.

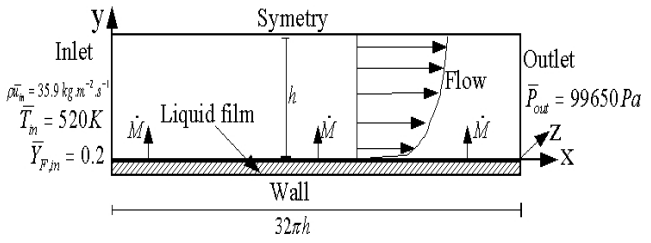

Figure 7: Computational domain for the IFP-C3D calculations.

Although the channel length shown in Figure 7 is longer than the one used for DNS calculations, the comparison of the results along the entire height of the channel is not easy to obtain. Indeed, the evaporation and heat flux in the liquid film prevent the boundary layer to be fully developed over a sufficiently wide part of the channel. It is why, the comparison of the RANS and the DNS results have been limited to the wall cell of the RANS channel in which the mean values of the temperature $\left\langle \overline{T} \right\rangle_m$, pressure $\left\langle \overline{P} \right\rangle_m$, fuel mass $\left\langle \rho \overline{Y}_F \right\rangle_m$ and the streamwise velocity $\overline{u}_m$ are the same as those given by the DNS. These conditions are summarized in Table 4.

Table 4: Space averaged DNS results on the entire height of the wall cell of the RANS grid.

$\left\langle \overline{P} \right\rangle_m = 99750Pa$	$\left\langle \overline{T} \right\rangle_m = 400.8K$
$\left\langle \rho \overline{Y}_F \right\rangle_m = 0.52\,kg.m^{-3}$	$\overline{u}_m = 35.9m.s^{-1}$

4.2 Results discussion

In this subsection, we compare the present model results with the DNS results and also with the OA liquid film evaporation model results as well implemented in IFP-C3D. The comparisons are made in terms of the friction velocity, heat and mass fluxes at the film interface (Tables 5 and 6). For each calculations (present model or OA model), the inlet boundary conditions of the channel were adjusted to obtain the Table 4 parameters values in the wall cell under study.

Table 5: Comparative results.

Variables	u_τ	φ_{gs}	$\dot{M}$
Units	$\left[m.s^{-1}\right]$	$\left[kJ.m^{-2}.s^{-1}\right]$	$\left[kg.m^{-2}.s^{-1}\right]$
DNS results	$1,52$	$24,4$	$9,63.10^{-2}$
Present Model	$1,54$	$22,8$	$9,17.10^{-2}$
OA Model	$2,62$	$34,3$	$4,49.10^{-2}$

Table 6: Per cent errors between RANS models and DNS results.

Variables	u_τ	φ_{gs}	$\dot{M}$
Present Model	$+1,3\%$	$-6,6\%$	$-4,8\%$
OA Model	$+72,4\%$	$+40,6\%$	$-53,4\%$

Tables 5 and 6 show that the results provided by the model presented in this paper are very close to the DNS results with a maximum error less than 7% for the interface heat flux. The differences observed seems to be mainly due to the fact that the profiles given by the wall laws are not exactly the same as those of the DNS (Figures 2,3,4). This may explain why the error gap is more significant for φ_{gs} and $\dot{M}$ than for u_τ. Indeed, the temperature and fuel mass fraction profiles are integrated in the wall cell which contains the buffer zone, for which the accuracy of the wall functions are the worst. However, the present evaporation model improves the accuracy of the wall laws results. Finally, one can note that the OA model results are relatively far from the DNS results. The friction velocity u_τ is overestimated which increases the heat flux and decreases the evaporated mass $\dot{M}$.

5. CONCLUSIONS

In this paper, a single component film evaporation model has been developed for wall temperature smaller than the saturation temperature of the liquid.

The model equations has been derived by assuming a third order temperature profile along the wall normal

direction. The transient heating stage of the film has been also taken into account.

An analytical wall-laws have been derived for a compressible and non-isothermal gas flow with strong density and viscosity gradients near an evaporating liquid film. The wall-laws coefficients including the laminar-turbulent transition positions have been fitted using DNS results.

The complete model have been implemented in the IFP-C3D code already including the liquid film OA model.

The new wall-laws results are shown to be in good agreement with the DNS results.

The validation of the complete evaporation model against experimental data is still necessary. This represent our future work although such experiments are very rare.

6. REFERENCES

1. Desoutter, G., Cuenot, B., Habchi, C. and Poinsot, T., Interaction of a Premixed Flame with a Liquid Fuel Film on a Wall, Proc. 30th International Symposium on Combustion, Proc. of the Combustion Institute 30, pp. 259-266, 2005.
2. Stanton, W. and Rutland, C.J., Modeling Fuel Film Formation and Wall Interaction in Diesel Engines, SAE, No. 960628, 1996.
3. Stanton, D.W., Lippert, A.M., Reitz, R.D. and Rutland, C.J., Influence of Spray-Wall Interaction and Fuel Films on Cold Starting in Direct Injection Diesel Engines, SAE, No. 982584, 1998.
4. Bai, C. and Gosman, A.D., Mathematical Modeling of Wall Films Formed by Impinging Sprays, SAE, No. 960626, 1996.
5. Foucart, H., Modélisation Tridimensionnelle des Films Liquides Pariétaux dans les Moteurs à Combustion Interne, PhD. thesis, University of Rouen, France, 1998.
6. Foucart, H., Habchi, C., Le Coz, J.-F., Baritaud, T., Development of a Three-Dimensionnal Model of Fuel Liquid Film for Internal Combustion Engines, SAE, No. 980133, 1998.
7. Han, Z., Xu, Z., Wall Film Dynamics Modeling for Impinging Sprays in Engines, SAE, No. 2004-01-0099, 2004.
8. O'Rourke, P.J. and Amsden, A.A., A Particle Numerical Model for Wall Film Dynamics in Port-Injected Engines, SAE, No. 961961, 1996.
9. O'Rourke, P.J. and Amsden, A.A., A Spray/Wall Interaction Submodel for the KIVA-3 Wall Film Model, SAE, No. 2000-01-0271, 2000.
10. Schönfeld, T. and Rudgyard, M., Steady and Unsteady Flows Simulations Using the Hybrid Flow Solver AVBP, AIAA Journal, Vol. 37, pp. 1378-1385, 1999.
11. Amsden, A.A., O'Rourke, P.J. and Butler, T.D., KIVA-II A Computer Program for Chemically Reactive Flows with Sprays, Los Alamos National Laboratory, Rept. LA-11560-MS, Los Alamos, New Mex., 1989.
12. Colin, O. and Rudgyard, M., Development of High-Order Taylor-Galerkin Schemes for Unsteady Calculations, Journal of Computational Physics, Vol. 162, pp. 338-371, 2000.
13. Jiménez, J. and Moin, M., The minimal Flow Unit in Near-Wall Turbulence, J. Fluid Mech., Vol. 225, pp. 213-240, 1991.
14. Ern, A. and Giovangigli, V., Multicomponent Transport Algorithms, In Verlag, S., editor, Lecture Notes in Physics, Springer Verlag, Heidelberg, 1994.
15. Angelberger, C., Contributions à la Modélisation de l'Interaction Flame-Paroi et Des Flux Pariétaux dans les Moteurs à Allumage Commandé, Ph.D. thesis, PSA Peugeot-Citoöen and Cerfacs, 1997.
16. Launder, B.E. and Spalding D.B., The Numerical Computation of Turbulent Flows, Computer Methods in Applied Mechanics and Engineering, Vol.3, pp. 269-289, 1974.
17. Réveillé B., Kleemann A., Knop V., and Habchi C., Potential of Narrow Angle Direct Injection Diesel Engines for Clean Combustion: 3D CFD Analysis, SAE paper 2006-01-1365.